

Natural and unnatural parity states of small trapped equal-mass two-component Fermi gases at unitarity and fourth-order virial coefficient

D. Rakshit,¹ K. M. Daily,¹ and D. Blume¹

¹*Department of Physics and Astronomy, Washington State University, Pullman, Washington 99164-2814, USA*

(Dated: August 16, 2018)

Equal-mass two-component Fermi gases under spherically symmetric external harmonic confinement with large s -wave scattering length are considered. Using the stochastic variational approach, we determine the lowest 286 and 164 relative eigenenergies of the (2, 2) and (3, 1) systems at unitarity as a function of the range r_0 of the underlying two-body potential and extrapolate to the $r_0 \rightarrow 0$ limit. Our calculations include all states with vanishing and finite angular momentum L (and natural and unnatural parity Π) with relative energy up to $10.5\hbar\Omega$, where Ω denotes the angular trapping frequency of the external confinement. Our extrapolated zero-range energies are estimated to have uncertainties of 0.1% or smaller. The (2, 2) and (3, 1) energies are used to determine the fourth-order virial coefficient of the trapped unitary two-component Fermi gas in the low-temperature regime. Our results are compared with recent predictions for the fourth-order virial coefficient of the homogeneous system. We also calculate small portions of the energy spectra of the (3, 2) and (4, 1) systems at unitarity.

PACS numbers:

I. INTRODUCTION

Small trapped Fermi gases with contact or short-range interactions have attracted a great deal of attention recently [1]. Using lithium or potassium, for example, equal-mass two-component systems can be realized experimentally by occupying two different hyperfine states. For typical experimental conditions, p -wave or higher partial wave interactions between two like atoms (say, two spin-up atoms) and between two unlike atoms (a spin-up and a spin-down atom) are negligibly small. Furthermore, by tuning an external magnetic field in the vicinity of a Fano-Feshbach resonance, the s -wave scattering length a_s can be adjusted to essentially any value [2]. In this paper, we consider the regime where the s -wave scattering length is much larger than the range r_0 of the underlying two-body model potential. In the limit that r_0 goes to zero and a_s goes to infinity, the unitary regime is realized. In this regime, the only meaningful length scale of the system is given by the oscillator length a_{ho} that characterizes the external confining potential [1, 3]. Throughout, we assume a spherically symmetric harmonic potential with angular trapping frequency Ω (i.e., $a_{\text{ho}} = \sqrt{\hbar/(m\Omega)}$ with m denoting the atom mass).

From a theoretical point of view, small harmonically trapped Fermi gases with central short-range interactions are particularly appealing since they can be treated with comparatively high accuracy by a variety of methods, including techniques that have been developed in the context of atomic physics, nuclear physics and quantum chemistry problems [4–16]. For the harmonically trapped equal-mass system, the center of mass degrees of freedom separate. Furthermore, the relative orbital angular momentum quantum number L , the projection quantum number M and the parity Π are good quantum numbers. This implies that the Hilbert space can be divided into

subspaces, which significantly reduces the complexity of the calculations compared to, for example, systems confined to move within a box with periodic boundary conditions [17]. The harmonically trapped Fermi gas consisting of two spin-up and two spin-down atoms with vanishing angular momentum has been treated by a variety of techniques in the literature (see Refs. [1, 18] for reviews). The ground state energy and ground state properties of the (2, 2) system in the zero-range limit, for example, are by now well characterized [5, 11]. Much less, however, is known about the excitation spectrum [5, 6, 12, 19], which contains both natural and unnatural parity states, i.e., states with parity $\Pi = (-1)^L$ and $\Pi = (-1)^{L+1}$, respectively. While a good portion of the excitation spectrum of the (2, 2) system with natural parity has been determined throughout the crossover and at unitarity [12], little is known about the properties of states with unnatural parity. Moreover, the energy spectra of the (3, 1), (3, 2) and (4, 1) systems have not yet been characterized in detail.

This paper presents extensive benchmark results for the (2, 2) and (3, 1) energies of natural and unnatural parity states at unitary. In addition, we present portions of the energy spectra of the (3, 2) and (4, 1) systems. We then use the energy spectra of the (2, 2) and (3, 1) systems at unitarity to determine the fourth-order virial coefficient b_4 of the trapped system in the low-temperature regime. The fourth-order virial coefficient enters into the virial equation of state, which allows for the determination of the universal thermodynamics of two-component Fermi gases in the temperature regime down to about half the Fermi temperature T_F [20–27]. For the temperature regime in which we have convergence, i.e., for $k_B T \lesssim 2\hbar\Omega/3$, where T denotes the temperature and k_B Boltzmann's constant, we find that the fourth-order virial coefficient b_4 of the trapped system is negative and decreases monotonically with increasing tempera-

ture. If we assume that b_4 continues to change monotonically with increasing temperature in the medium- and high-temperature regime, our results predict that the fourth-order virial coefficient of the trapped system and—through application of the local density approximation (LDA)—that of the homogeneous system approach a negative value in the high-temperature limit. This is in contrast to recent results [26–28] based on the equation of state, determined both experimentally and calculated via a diagrammatic Monte Carlo technique. These studies predict that the fourth-order virial coefficient of the homogeneous system is positive. The discrepancy would be resolved if the fourth-order virial coefficient of the trapped system was changing non-monotonically with temperature, allowing for a sign change of b_4 in the medium- or high-temperature regime. Analogous non-monotonic behavior was found for one of the third-order virial coefficients of the trapped unequal-mass two-component Fermi gas at unitarity [29]. While we do not have access to sufficiently large portions of the energy spectra of the (2, 2) and (3, 1) systems to determine the fourth-order virial coefficient of the trapped system in the medium- and high-temperature regimes (thereby preventing us from drawing definite conclusions), our results illuminate a number of aspects related to the determination of the virial coefficients from few-body energy spectra.

Section II introduces the system under study, reviews the stochastic variational approach, and presents details regarding our implementation. Compact expressions for the relevant matrix elements for natural and unnatural parity states are presented in Appendix A. Section III (see also supplementary material [30]) summarizes our extrapolated zero-range energies for the (2, 2), (3, 1), (3, 2) and (4, 1) systems in tabular form and discusses their characteristics. Section IV uses the (2, 2) and (3, 1) energies to determine the fourth-order virial coefficient of the trapped system at unitarity. Lastly, Sec. V concludes.

II. SYSTEM UNDER STUDY AND STOCHASTIC VARIATIONAL APPROACH

We consider a two-component Fermi gas with n_1 spin-up and n_2 spin-down atoms of mass m with $n = n_1 + n_2$. We assume that the atoms are confined by a spherically symmetric trapping potential with angular frequency Ω . Furthermore, we assume that the spin-up and spin-down atoms interact through a short-range interaction potential $V_{\text{tb}}(r_{pq})$, where \vec{r}_p ($p = 1, \dots, n$) denotes the position vector of the p^{th} atom measured relative to the center of the trap and $r_{pq} = |\vec{r}_p - \vec{r}_q|$, and that atoms with like spins do not interact. The model Hamiltonian H then reads

$$H = \sum_{p=1}^n \left(\frac{-\hbar^2}{2m} \nabla_{\vec{r}_p}^2 + \frac{1}{2} m \Omega^2 r_p^2 \right) + V_{\text{int}}, \quad (1)$$

where

$$V_{\text{int}} = \sum_{p=1}^{n_1} \sum_{q=n_1+1}^n V_{\text{tb}}(r_{pq}). \quad (2)$$

Throughout, we are interested in the regime where the s -wave scattering length a_s of the interspecies interaction potential V_{tb} becomes infinitely large. For the $(n_1, n_2) = (1, 1)$ and $(2, 1)$ systems, semi-analytical solutions are known if V_{tb} coincides with the zero-range δ -function potential [4, 31]. For (n_1, n_2) systems with $n_1 + n_2 \geq 4$, however, no such semi-analytical solutions are known. To determine the eigenenergies of (n_1, n_2) systems with $n_1 + n_2 = 4$ and 5, we separate off the center of mass motion and resort to a numerical technique, the stochastic variational approach [32]. In this approach, it is convenient to model the interactions between the unlike atoms through a Gaussian potential $V_g(r)$ with depth $-V_0$ ($V_0 > 0$) and range r_0 [5],

$$V_g(r) = -V_0 \exp \left[- \left(\frac{r}{\sqrt{2}r_0} \right)^2 \right]. \quad (3)$$

To treat the unitary system, we adjust the depth V_0 of V_g for a given r_0 such that the two-body system in free space supports one zero-energy s -wave bound state but no deep-lying bound states. To determine the zero-range energies, we consider a number of r_0 , $r_0 \ll a_{\text{ho}}$, and extrapolate the finite-range energies to the $r_0 \rightarrow 0$ limit (see Sec. III for examples).

We take advantage of the fact that the Hamiltonian H separates into the center of mass Hamiltonian H^{cm} and the relative Hamiltonian H^{rel} , $H = H^{\text{rel}} + H^{\text{cm}}$. In the following, we consider the relative Hamiltonian H^{rel} and use the stochastic variational approach to determine the eigenenergies and eigenstates of the Schrödinger equation $H^{\text{rel}}\Psi^{\text{rel}} = E_{n_1, n_2}^{\text{rel}}\Psi^{\text{rel}}$. Here, we explicitly indicate the dependence of the eigenenergies on n_1 and n_2 but, for notational simplicity, not that of the Hamiltonian and the wave function. To compact the notation, we write H^{rel} as $H^{\text{rel}} = T^{\text{rel}} + V_{\text{trap}}^{\text{rel}} + V_{\text{int}}$, where T^{rel} denotes the kinetic energy operator associated with the relative motion, and $V_{\text{trap}}^{\text{rel}}$ the contribution of the confining potential associated with the relative degrees of freedom.

The stochastic variational approach is a basis set expansion approach that writes the relative wave function Ψ^{rel} of a given state in terms of a set of basis functions ψ_k [32],

$$\Psi^{\text{rel}} = \sum_{k=1}^{N_b} c_k \mathcal{A} \psi_k. \quad (4)$$

Here, the c_k denote expansion coefficients and \mathcal{A} an anti-symmetrization operator that ensures that the wave function is anti-symmetric under the exchange of any pair of like fermions. In Eq. (4), N_b denotes the number of basis functions. As with other basis set expansion approaches,

the Ritz variational principle ensures that the lowest energy as well as the higher-lying energies obtained by the stochastic variational approach are rigorous upper bounds to the exact eigenenergies of the system [32]. In the following, we introduce the basis functions used in this work, which have good orbital angular momentum L , projection quantum number M and parity Π ; here, L , M and Π are associated with the relative motion.

Following Refs. [32–38], we write the basis functions ψ_k as a product of a correlated Gaussian [second line of Eq. (5)] and a “prefactor” [first line of Eq. (5)] that carries the angular momentum L of the system,

$$\psi_k(\vec{x}) = |\vec{v}_{1k}|^{l_1} |\vec{v}_{2k}|^{l_2} [Y_{l_1}(\hat{v}_{1k}) \otimes Y_{l_2}(\hat{v}_{2k})]_{LM} \times \exp\left(-\frac{\vec{x}^T \underline{A}_k \vec{x}}{2}\right). \quad (5)$$

Here, \vec{x} collectively denotes the $n - 1$ Jacobi vectors $\vec{\rho}_p$, where $p = 1, \dots, n - 1$. The notation $[Y_{l_1}(\hat{v}_{1k}) \otimes Y_{l_2}(\hat{v}_{2k})]_{LM}$ indicates that the spherical harmonics $Y_{l_1 m_1}$ and $Y_{l_2 m_2}$ are coupled to form a function with angular momentum L and projection quantum number M . For states with natural parity, i.e., for states whose parity is given by $\Pi = (-1)^L$, we choose $l_1 = L$ and $l_2 = 0$ [32–35]. For states with unnatural parity ($L > 0$), i.e., for states whose parity is given by $\Pi = (-1)^{L+1}$, we choose $l_1 = L$ and $l_2 = 1$ [36, 37]. The basis functions that describe unnatural parity states with $L = 0$ have a slightly different form since the construction of states with $L = 0$ and $\Pi = -1$ requires the coupling of three spherical harmonics with l_1, l_2 and $l_3 > 0$ [36, 38]. The matrix \underline{A}_k is symmetric and positive-definite, and has dimensions $(n - 1) \times (n - 1)$. The $n(n - 1)/2$ independent elements of \underline{A}_k are treated as variational parameters and optimized semi-stochastically. The three-dimensional vectors \vec{v}_{1k} and \vec{v}_{2k} , referred to as global vectors since they depend on all $n - 1$ Jacobi vectors, are defined through $\vec{v}_{1k} = \sum_{p=1}^{n-1} u_{1k,p} \vec{\rho}_p = \vec{u}_{1k}^T \vec{x}$ and similarly for \vec{v}_{2k} . The vectors \vec{u}_{1k} and \vec{u}_{2k} are optimized semi-stochastically, where $\vec{u}_{1k} = (u_{1k,1}, \dots, u_{1k,n-1})$ and similarly for \vec{u}_{2k} .

A key benefit of the basis functions given in Eq. (5) is that the overlap matrix element $O_{k'k} = \langle \psi_{k'} | \psi_k \rangle$, the matrix element for the kinetic energy operator $(T^{\text{rel}})_{k'k} = \langle \psi_{k'} | T^{\text{rel}} | \psi_k \rangle$, and the matrix element for the confining potential $(V_{\text{trap}}^{\text{rel}})_{k'k} = \langle \psi_{k'} | V_{\text{trap}}^{\text{rel}} | \psi_k \rangle$ reduce to compact expressions [32–37]. Here, it is understood that the integration is performed over all $3n - 3$ Jacobi coordinates and that ψ_k is characterized by $\underline{A}_k, \vec{u}_{1k}$ and \vec{u}_{2k} while $\psi_{k'}$ is characterized by $\underline{A}_{k'}, \vec{u}_{1k'}$ and $\vec{u}_{2k'}$. Moreover, a compact expression can also be found for the matrix elements $(V_{\text{int}})_{k'k} = \langle \psi_{k'} | V_{\text{int}} | \psi_k \rangle$ associated with the atom-atom interaction if V_{tb} is modeled by the Gaussian potential V_g . Appendix A summarizes explicit expressions of the matrix elements with natural parity (any L) and unnatural parity ($L > 0$). The matrix elements for states with 0^- symmetry can be found in Refs. [36, 38].

We note that the overlap matrix element $O_{k'k}$ between two different basis functions does not vanish, i.e., the basis set employed is not orthogonal. This implies that the

determination of the eigenenergies amounts to the diagonalization of a generalized eigenvalue problem defined by the Hamiltonian and overlap matrices [32]. While one might think, at first sight, that the non-orthogonality of the basis functions could introduce numerical instabilities, it has been shown in previous work [5, 6, 9, 12, 14] that numerical instabilities due to linear dependence issues can be avoided completely for the systems of interest in this work if the basis sets are chosen carefully.

Our strategy to optimize the large number of non-linear variational parameters is quite simple [32]. We start with a reference basis set, which could consist of just one basis function or as many as several 100 or 1000 basis functions. We then enlarge this reference basis set by one basis function, which is chosen from a large number of trial basis functions, typically between several 100 and several 1000. Each trial function is characterized by a different set of variational parameters. To decide which trial basis function to keep, we calculate the energy for each of the enlarged trial basis sets, which consist of the reference basis set plus one of the trial basis functions, and choose the one that results in the largest reduction of the energy of the state of interest. The state of interest could be the ground state or an excited state. The procedure is repeated till the basis set is sufficiently complete to describe the state of interest with the desired accuracy.

When optimizing a state whose energy is nearly degenerate with that of another state or when optimizing highly excited states, some care needs to be exercised. In the former case, we find it advantageous to optimize two or more states simultaneously. In the latter case, we find it beneficial to start with a basis set that provides a reasonably accurate description of the lower lying part of the energy spectrum. The advantage of our optimization procedure is that the basis set is optimized for a particular state or a particular subset of states. Correspondingly, we work with comparatively small basis sets. The energies of the (2, 2) and (3, 1) systems at unitarity (see Table I and supplemental material) are obtained using basis sets that consist of 700-3400 basis functions, while the energies of the (3, 2) and (4, 1) systems (see supplemental material) are obtained using basis sets that consist of 1500-3800 basis functions.

III. ENERGIES OF SMALL TRAPPED FERMI GASES

One key purpose of this paper is to elucidate how we determine a large portion of the energy spectrum of trapped two-component Fermi systems with $n = 4$ and 5, and to tabulate the extrapolated zero-range energies. We believe that the tabulation of the energies is useful as these energies provide much needed highly accurate benchmark results that can be used to assess the accuracy and validity regime of alternative approaches. We anticipate that the tabulated energies will also prove useful in other applications.

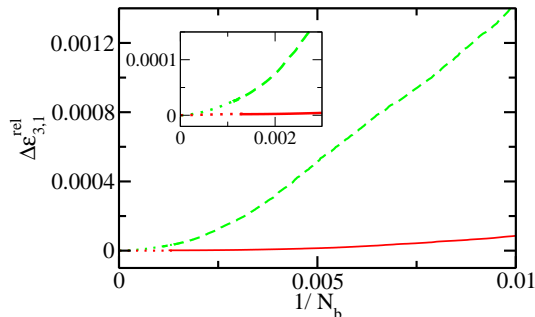


FIG. 1: (Color online) Illustration of convergence for the (3, 1) system at unitarity with 1^+ symmetry and $r_0 = 0.04a_{\text{ho}}$. Solid and dashed lines show the quantity $\Delta\epsilon_{3,1}^{\text{rel}}$, where $\Delta\epsilon_{3,1}^{\text{rel}} = [E_{3,1}^{\text{rel}}(N_b) - E_{3,1}^{\text{rel}}(N_b \rightarrow \infty)]/E_{3,1}^{\text{rel}}(N_b \rightarrow \infty)$, for states 1 and 12 as a function of $1/N_b$. Dotted lines show the extrapolation to the $N_b \rightarrow \infty$ limit. The inset shows a blow-up of the small $1/N_b$ region.

Figure 1 shows an example of our basis set optimization for the (3, 1) system with 1^+ symmetry and $r_0 = 0.04a_{\text{ho}}$ at unitarity. Solid and dashed lines show the fractional difference $\Delta\epsilon_{3,1}^{\text{rel}}$ for the ground state (state 1) and state 12 [39], respectively, between the relative energy $E_{3,1}^{\text{rel}}$ for a basis set of size N_b and the energy for an infinite basis set. The dotted lines in Fig. 1 show the extrapolation to the $N_b \rightarrow \infty$ limit. It can be seen that the ground state energy converges notably faster than the excited state energy. The energies for $N_b = 800$ and $N_b = 900$ are $E_{3,1}^{\text{rel}}(r_0 = 0.04a_{\text{ho}}) = 5.08294\hbar\Omega$ for state 1 and $E_{3,1}^{\text{rel}}(r_0 = 0.04a_{\text{ho}}) = 10.1788\hbar\Omega$ for state 12, respectively. The basis set errors for these basis sizes are 0.0002% and 0.003%, respectively, i.e., the energies of states 1 and 12 lie respectively 0.00001 $\hbar\Omega$ and 0.0003 $\hbar\Omega$ above the extrapolated energies for the infinite basis set. The low-lying states of the (3, 1) system with 1^+ symmetry at unitarity converge relatively quickly with increasing N_b . The convergence is slower for most other states and, in general, we choose the size of our basis sets for the (2, 2) and (3, 1) systems such that the basis set extrapolation error is smaller than 0.1 %.

Figure 2 exemplarily illustrates the range dependence for the relative energy of the (3, 1) system with 1^+ symmetry. Figure 2(a) shows the range dependence of the ground state energy, Fig. 2(b) shows the range dependence of the energy associated with state 12, and Fig. 2(c) shows the range dependence of the energy for a state that depends comparatively weakly on r_0 (state 5). In Figs. 2(a) and 2(b), the energies vary to a very good approximation linearly with r_0 for sufficiently small r_0/a_{ho} . This finding is in agreement with earlier work [9, 11, 12, 14]. For the ground state [see Fig. 2(a)], the range dependence is quite weak and linear behavior is only observed for $r_0 \lesssim 0.03a_{\text{ho}}$.

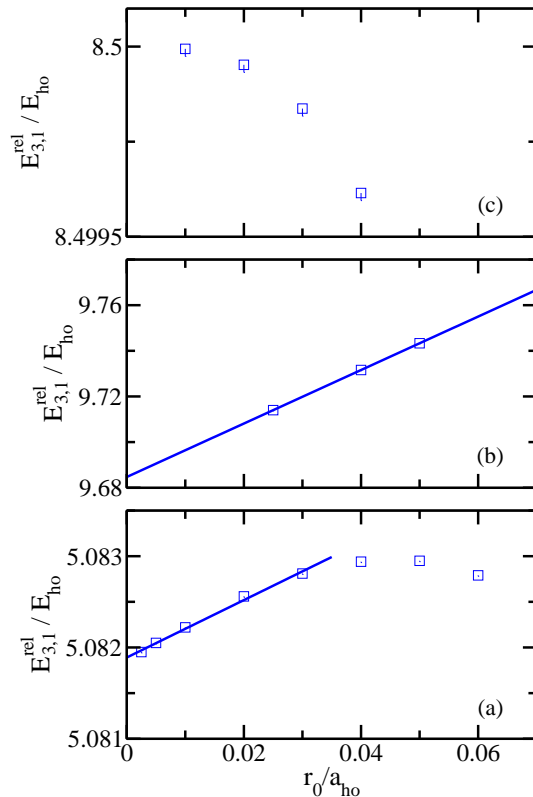


FIG. 2: (Color online) Illustration of finite-range dependence for the (3, 1) system with 1^+ symmetry at unitarity. Squares show the relative eigenenergies $E_{3,1}^{\text{rel}}(N_b)$ for various ranges r_0 of the underlying two-body interaction potential for (a) the ground state (state 1), (b) state 12, and (c) state 5; N_b is the largest basis set considered. The energies provide variational upper bounds and the estimated basis set extrapolation error is indicated by errorbars; in panels (a) and (b), the basis set extrapolation error is smaller than the symbol size and thus not visible. In panels (a) and (b), solid lines show linear fits to the energies $E_{3,1}^{\text{rel}}(N_b)$ [the fit shown in panel (a) includes the energies for the five smallest r_0 values].

In Fig. 2(c), the zero-range energy agrees to within 0.00002 $\hbar\Omega$ with the energy of the non-interacting system. This, combined with the very weak dependence of the energy on r_0 and the fact that the energy approaches the zero-range limit from below, suggests that this state is not affected by s -wave scattering but only by higher-partial wave scattering. In the zero-range limit, energy shifts associated with higher-partial wave scattering processes vanish. Our interpretation is corroborated by a perturbative calculation along the lines of that performed in Refs. [9, 12], which utilizes zero-range contact interactions. For the (3, 1) system with $L^\Pi = 1^+$ symmetry, we find, in agreement with our results based on the stochastic variational approach, that there exists one state with relative energy $17\hbar\Omega/2$ and six states with relative energy

$21\hbar\Omega/2$ that are independent of a_s .

We refer to states that are unaffected by s -wave interactions as unshifted states. We find that a relatively large number of states fall into this category. Their existence and likelihood of occurrence has already been discussed for the (2, 1) and (2, 2) systems in the literature [4, 12]. For the (2, 1) system, e.g., all unnatural parity states are unaffected by s -wave interactions in the zero-range limit. For the (2, 2) and (3, 1) systems, unnatural parity states can be affected by s -wave interactions in the zero-range limit. The only exception are states with 0^- symmetry, which are unshifted. This behavior can be intuitively understood within a picture that utilizes angular momentum coupling. To construct a state with 0^- symmetry, the coupling of three finite angular momenta is needed. These angular momenta can be envisioned as being each associated with one of the three Jacobi vectors that characterize the $n = 4$ system. As a consequence, the s -wave interactions are effectively turned off by the nodal structure of the wave function. For $n = 5$, this argument predicts that states with 0^- symmetry can be affected by s -wave interactions since the system is characterized by one more Jacobi vector than angular momenta needed to ensure the 0^- symmetry. Indeed, this prediction is in agreement with our results from the perturbative and stochastic variational calculations.

Table I summarizes our extrapolated zero-range energies $E_{3,1}^{\text{rel}}(r_0 = 0)$, $E_{3,1}^{\text{rel}}(r_0 = 0) \leq 10.5\hbar\Omega$, for states with 1^+ symmetry at unitarity that are affected by s -wave interactions. The zero-range energies are obtained by calculating the energies of a given state for several ranges r_0 between $0.0025 \leq r_0/a_{\text{ho}} \leq 0.08$ and by then fitting these energies for the largest basis set considered by a linear function. The third column in Table I shows the slopes χ , which characterize the dependence of $E_{3,1}^{\text{rel}}$ on r_0 at unitarity. We find that the slopes for states that are affected by s -wave interactions are positive. Table I shows that the slopes vary over nearly two orders of magnitude. The slopes can be related to the effective range r_{eff} using the relation $r_{\text{eff}} = 2.032r_0$. This numerically determined relationship is specific to the Gaussian model potential employed in this paper and is quite accurate over the r_0 values considered. It may be used to estimate the leading order dependence of the energies on the effective range for the Gaussian model potential.

The relative energies at unitarity for zero-range interactions can be written in the form $(2q + s_{L,\nu} + 1)\hbar\Omega$ [4, 40], where $s_{L,\nu}$ is associated with the eigenvalue of the hyperangular Schrödinger equation and where the radial quantum number q takes the values $0, 1, \dots$ (although the $s_{L,\nu}$ depend on Π , this dependence is not explicitly indicated for notational simplicity). The fourth column of Table I shows the $s_{L,\nu}$ values determined from our energies for $q = 0$, i.e., for the lowest rung of the ladder with $2q\hbar\Omega$ spacings. The extrapolated zero-range energies of states 2 and 7, e.g., lie $2.0001\hbar\Omega$ and $4.0006\hbar\Omega$, respectively, above the energy of the ground state. Correspondingly, we assign the quantum numbers $q = 1$ and $q = 2$ to these

TABLE I: Relative energies $E_{3,1}^{\text{rel}}$ for the (3, 1) system with $L^\Pi = 1^+$ symmetry [only states that are affected by s -wave interactions are included; each energy is $(2L + 1)$ -fold degenerate]. The first column indicates the state number (st. no.). The second column shows the extrapolated zero-range energy $E_{3,1}^{\text{rel}}(r_0 = 0)$ at unitarity; the uncertainty is estimated to be 0.1 % or smaller. The third column indicates the dependence of the energy at unitarity on the range r_0 of the Gaussian potential V_g . We assume a linear dependence and write $E_{3,1}^{\text{rel}}(r_0) = E_{3,1}^{\text{rel}}(r_0 = 0) + \chi(r_0/a_{\text{ho}})\hbar\Omega$. The fourth column shows the $s_{L,\nu}$ value determined from the energy; the value of $s_{L,\nu}$ is only shown for the lowest rung of a ladder, i.e., for states with $q = 0$. The last column shows $s_{L,\nu}^{\text{ni}}$ of the non-interacting state that is “paired” with the interacting state when determining $\Delta Q_{3,1}$ (see Sec. IV). There exist 1 and 6 unshifted states with energy $17\hbar\Omega/2$ and $21\hbar\Omega/2$, respectively.

st. no.	$E_{3,1}^{\text{rel}}(r_0 = 0)/(\hbar\Omega)$	χ	$s_{L,\nu}$	$s_{L,\nu}^{\text{ni}}$
1	5.0819	0.04	4.0819	5.5
2	7.0820	0.03		
3	7.6056	0.51	6.6056	7.5
4	8.1456	0.76	7.1456	7.5
6	8.9846	1.19	7.9846	9.5
7	9.0825	0.03		
8	9.1324	0.28	8.1324	9.5
9	9.4544	0.46	8.4544	9.5
10	9.6060	0.55		
11	9.6847	1.17	8.6847	9.5
12	10.147	0.80		

states, i.e., we identify them as belonging to the same ladder as the ground state. The small deviations from the $2q\hbar\Omega$ spacings can be interpreted as a measure of our numerical accuracy. For the states considered in Table I, the $2q\hbar\Omega$ spacing is fulfilled to better than 0.1 %. We find that the energies of states that belong to the same ladder are characterized by similar slopes.

For some symmetries, nearly degenerate states exist in the energy range $E^{\text{rel}} \leq 10.5\hbar\Omega$. Figure 3 shows the range dependence of the (3, 1) energies with 3^- symmetry corresponding to states 15 and 16. This figure illustrates exemplarily that the “ordering” of states can change as a function of r_0 , i.e., that the energies of two or more states can cross at finite r_0 . Crossings like these can only be resolved by considering at least three different r_0 values for each state.

Following the format of Table I, the supplemental material tabulates the energies of the (2, 2) and (3, 1) systems. The results are obtained by analyzing the finite-range energies determined by the stochastic variational approach along the lines discussed above. For the (2, 2) and (3, 1) systems, there exist 286 and 164 states at unitarity with relative energy $E_{n_1, n_2}^{\text{rel}}$ smaller or equal to $10.5\hbar\Omega$ [not counting the $(2L + 1)$ multiplicity]. Of these states, respectively 52 and 46 are unshifted. The

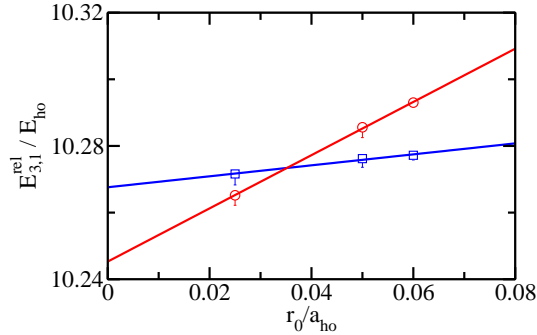


FIG. 3: (Color online) Illustration of finite-range dependence for (3,1) system with 3^- symmetry at unitarity. Circles and squares show the relative eigenenergies $E_{3,1}^{\text{rel}}(N_b)$ for states 15 and 16, respectively, for three different ranges r_0 of the underlying two-body interaction potential; N_b is the largest basis set considered (typically, N_b increases with decreasing r_0/a_{ho}). The energies provide variational upper bounds and the estimated basis set extrapolation error is indicated by errorbars. Solid lines show linear fits to the energies $E_{3,1}^{\text{rel}}(N_b)$.

shifted energies are characterized by respectively 170 and 89 $s_{L,\nu}$ values. Figures 4(a) and 4(b) show the density of states of the (2,2) system and the (3,1) system, respectively, at unitarity. The plots account for the $(2L+1)$ -multiplicity, and the density of states is shown separately for the shifted and unshifted states. It can be seen that the density of states increases significantly with increasing energy for both the (2,2) and (3,1) systems.

The supplemental material also tabulates results for the (3,2) and (4,1) systems. For these systems, the convergence is slower than for the $n=4$ systems, and we choose the size of our basis sets such that the basis set extrapolation error is smaller than 1%. Since the calculations for $n=5$ are significantly more demanding than for $n=4$, we restrict ourselves to states with $E_{n_1,n_2}^{\text{rel}} \lesssim 17\hbar\Omega/2$. We first extrapolate the energy for a given r_0 to the infinite basis set limit, and then determine the zero-range energy from these extrapolated energies. For the (3,2) and (4,1) systems, there exist 19 and 4 states with energies $E_{n_1,n_2}^{\text{rel}} \lesssim 17\hbar\Omega/2$ at unitarity [not counting the $(2L+1)$ multiplicity and excluding, for technical reasons, (3,2) states with 0^- symmetry]. All of these energies correspond to shifted states. One of the (3,2) energies corresponds to a “repeated state” with hyperradial quantum number $q=1$.

IV. 4th-ORDER VIRIAL COEFFICIENT

This section uses the (2,2) and (3,1) energies to determine the fourth-order virial coefficient b_4 of the s -wave interacting two-component Fermi gas under spherically symmetric harmonic confinement at unitarity in the low-

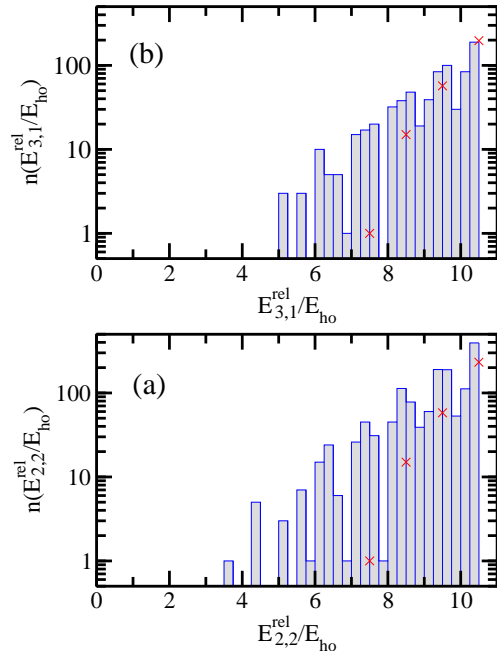


FIG. 4: (Color online) Panels (a) and (b) show the density of states for the (2,2) and (3,1) systems at unitarity; only the relative degrees of freedom are accounted for. The histograms show the number of energies corresponding to shifted states per $\hbar\Omega/4$ while the crosses show the number of energies corresponding to unshifted states. The histograms and the crosses account for the $(2L+1)$ -multiplicity of the energies.

temperature regime. We also summarize a few results for the low-temperature behavior of the higher-order virial coefficients.

The virial coefficients b_n enter into the virial equation of state, which describes the finite temperature behavior of trapped two-component Fermi gases [20–27, 29, 41–43]. We work in the grand canonical ensemble and denote the fugacities of component 1 and component 2 by z_1 and z_2 , respectively, where the z_i are defined in terms of the chemical potentials μ_i of the i th component and the temperature T ,

$$z_i = \exp[\mu_i/(k_B T)]. \quad (6)$$

The thermodynamic potential $\Omega^{(2)}$ of the harmonically trapped Fermi gas can be written in terms of the thermodynamic potentials $\Omega_1^{(1)}$ and $\Omega_2^{(1)}$ of the non-interacting components 1 and 2, and an “interaction piece” $\Delta\Omega^{(2)}$ that accounts for the interactions between the atoms of component 1 and the atoms of component 2 [23, 29, 41–43],

$$\Delta\Omega^{(2)} = -k_B T Q_1 \left(\sum_{n_1=1}^{\infty} \sum_{n_2=1}^{\infty} b_{n_1,n_2} z_1^{n_1} z_2^{n_2} \right). \quad (7)$$

TABLE II: The second and third columns show the expressions for $Q_1 \Delta b_n$ and b_n^{ref} , $n = 2-5$, for the trapped system. In deriving these expressions, we used that $\Delta Q_{n_1, n_2} = \Delta Q_{n_2, n_1}$ for the systems considered in this paper.

n	$Q_1 \Delta b_n$	b_n^{ref}
2	$\Delta Q_{1,1}/2$	0
3	$\Delta Q_{2,1}$	$-2b_2 Q_1$
4	$\Delta Q_{3,1} + \Delta Q_{2,2}/2$	$-b_2[(Q_1)^2 + b_2 Q_1 + 2Q_2] - 2b_3 Q_1$
5	$\Delta Q_{4,1} + \Delta Q_{3,2}$	$-2b_2[b_2(Q_1)^2 + Q_1 Q_2 + Q_3]$ $-b_3[(Q_1)^2 + 2Q_2 + 2b_2 Q_1] - 2b_4 Q_1$

In Eq. (7), Q_1 denotes the canonical partition function of a single particle in a spherically symmetric harmonic trap with angular frequency Ω ,

$$Q_1 = e^{3\tilde{\omega}/2} (e^{\tilde{\omega}} - 1)^{-3}, \quad (8)$$

where $\tilde{\omega}$ denotes a dimensionless inverse temperature,

$$\tilde{\omega} = \frac{\hbar\Omega}{k_B T}. \quad (9)$$

If we restrict ourselves to spin-balanced systems with equal masses, the fugacities z_1 and z_2 are equal, $z = z_1 = z_2$, and Eq. (7) reduces to

$$\Delta\Omega^{(2)} = -2k_B T Q_1 \left(\sum_{n=2}^{\infty} b_n z^n \right), \quad (10)$$

where $b_2 = b_{1,1}/2$, $b_3 = (b_{1,2} + b_{2,1})/2$, $b_4 = (b_{1,3} + b_{3,1} + b_{2,2})/2$, and so on.

We find it convenient to write the virial coefficients b_n as

$$b_n = \Delta b_n + b_n^{\text{ref}}, \quad (11)$$

where b_n^{ref} is determined by the virial coefficients b_j and the canonical partition functions Q_j with $j < n$. The interaction piece Δb_n , in contrast, accounts for the “new” physics introduced by the interacting (n_1, n_2) clusters with $n = n_1 + n_2$. Explicit expressions for Δb_n and b_n^{ref} are given in Table II, where the $\Delta Q_{n_1, n_2}$ are defined in terms of the canonical partition functions $Q_{n_1, n_2}^{\text{int}}$ and Q_{n_1} of the interacting (n_1, n_2) system and the single-component system with n_1 atoms, respectively,

$$\Delta Q_{n_1, n_2} = Q_{n_1, n_2}^{\text{int}} - Q_{n_1} Q_{n_2}. \quad (12)$$

The temperature-dependent canonical partition functions $Q_{n_1, n_2}^{\text{int}}$ and Q_{n_1} ,

$$Q_{n_1, n_2}^{\text{int}} = \sum_j \exp[-E_{n_1, n_2}^{\text{int}, j} / (k_B T)] \quad (13)$$

and

$$Q_{n_1} = \sum_j \exp[-E_{n_1}^{\text{ni}, j} / (k_B T)], \quad (14)$$

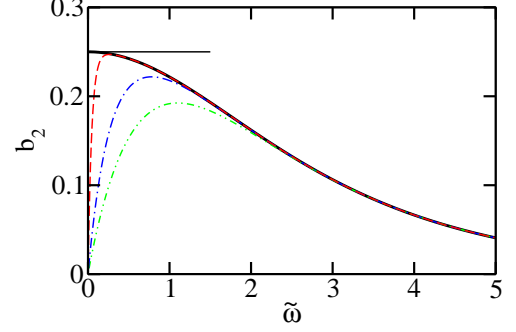


FIG. 5: (Color online) Virial coefficient b_2 of the trapped two-component Fermi gas at unitarity as a function of the inverse temperature $\tilde{\omega}$. The solid line shows b_2 , Eq. (17), while the dash-dot-dotted, dash-dotted and dashed lines show b_2 obtained by setting q_{max} in Eq. (16) to 0, 1 and 10, respectively. The solid horizontal line shows the high-temperature limit $b_2^{(0)}$.

are determined by the total energies $E_{n_1, n_2}^{\text{int}, j}$ and $E_{n_1}^{\text{ni}, j}$ of the interacting two-component and non-interacting single-component systems, respectively. It is important to note that the energies $E_{n_1, n_2}^{\text{int}, j}$ and $E_{n_1}^{\text{ni}, j}$ contain the center of mass energy. The summation over j in Eqs. (13) and (14) extends over all states allowed by symmetry. For $n_1 = 1$, the sum in Eq. (14) can be performed analytically, yielding Eq. (8). In the high-temperature limit, one finds for systems with zero-range interactions at unitarity that [23]

$$b_n = b_n^{(0)} + b_n^{(2)} \tilde{\omega}^2 + b_n^{(4)} \tilde{\omega}^4 + \dots \quad (15)$$

The second-order virial coefficient of the trapped system at unitarity takes the simple form [23]

$$b_2 = \Delta b_2 = \lim_{q_{\text{max}} \rightarrow \infty} \sum_{q=0}^{q_{\text{max}}} \frac{1}{2} [e^{-(2q+1/2)\tilde{\omega}} - e^{-(2q+3/2)\tilde{\omega}}] \quad (16)$$

or, performing the infinite sum,

$$b_2 = \frac{1}{2} e^{-\tilde{\omega}/2} (1 + e^{-\tilde{\omega}})^{-1}. \quad (17)$$

The solid line in Fig. 5 shows the second-order virial coefficient b_2 , Eq. (17), as a function of $\tilde{\omega}$. In the high-temperature (small $\tilde{\omega}$) limit, b_2 approaches the constant $b_2^{(0)}$, $b_2^{(0)} = 1/4$ (solid horizontal line in Fig. 5), which can be obtained by Taylor-expanding Eq. (17). To illustrate the convergence of b_2 with increasing energy cutoff, dash-dot-dotted, dash-dotted and dashed lines show b_2 obtained by setting q_{max} in Eq. (16) to 0, 1 and 10, respectively. For a finite energy cutoff, it can be seen that b_2 goes to 0 in the small $\tilde{\omega}$ region as opposed to $b_2^{(0)} = 1/4$.

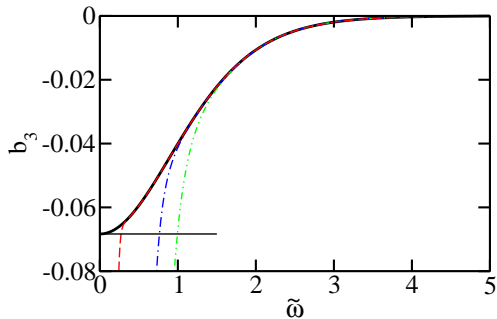


FIG. 6: (Color online) Virial coefficient b_3 of the trapped two-component Fermi gas at unitarity as a function of the inverse temperature $\tilde{\omega}$. The solid line shows b_3 with L_{\max} and ν_{\max} set to very large values (see Ref. [29] for details) while the dash-dot-dotted, dash-dotted and dashed lines show b_3 obtained by limiting L_{\max} and ν_{\max} in Eq. (18) such that $s_{L,\nu} \leq 11/2$, $\leq 19/2$ and ≤ 50 , respectively. The solid horizontal line shows the high-temperature limit $b_3^{(0)}$, Eq. (19).

As expected, a larger energy cutoff provides an accurate description of b_2 over a larger temperature range, i.e., down to a smaller inverse temperature $\tilde{\omega}$.

The relative three-body energies at unitarity and for vanishing s -wave scattering length a_s can be written as $(2q + s_{L,\nu} + 1)\hbar\Omega$ (see Sec. III) and $(2q + s_{L,\nu}^{\text{ni}} + 1)\hbar\Omega$, respectively. Performing the sum over q analytically, the interaction piece Δb_3 of the trapped three-body system at unitarity takes the form [23, 29]

$$\Delta b_3 = \lim_{\nu_{\max}, L_{\max} \rightarrow \infty} e^{2\tilde{\omega}} (e^{2\tilde{\omega}} - 1)^{-1} \times \sum_{\nu=0}^{\nu_{\max}} \sum_{L=0}^{L_{\max}} (2L+1) [e^{-(s_{L,\nu}+1)\tilde{\omega}} - e^{-(s_{L,\nu}^{\text{ni}}+1)\tilde{\omega}}]. \quad (18)$$

Using large L_{\max} and ν_{\max} , a fully converged pointwise representation of b_3 is obtained [23, 29] (see solid line in Fig. 6). Using the analytical forms for Q_1 and b_2 , Eqs. (8) and (17), we find that b_3^{ref} diverges as $-\tilde{\omega}^{-3}/2 + \tilde{\omega}^{-1}/8$ in the high-temperature limit. This divergence is cancelled by a divergence of Δb_3 of opposite sign. As a result, b_3 is well behaved in the small $\tilde{\omega}$ (high T) limit. A careful analysis of the high-temperature behavior gives [23, 29]

$$b_3^{(0)} = -0.0683396093112849(1) \quad (19)$$

(see horizontal solid line in Fig. 6).

To illustrate the convergence of b_3 with increasing L_{\max} and ν_{\max} [see Eq. (18)], dash-dot-dotted, dash-dotted and dashed lines in Fig. 6 show b_3 calculated using Δb_3 from Eq. (18) with L_{\max} and ν_{\max} chosen such that $s_{L,\nu} \leq 11/5$, $\leq 19/5$ and ≤ 50 , respectively. No cutoff is imposed in calculating b_3^{ref} . In these calculations, we include the same number of $s_{L,\nu}$ and $s_{L,\nu}^{\text{ni}}$ in evaluating Δb_3 , i.e., each interacting $s_{L,\nu}$ value is paired with the corresponding non-interacting $s_{L,\nu}^{\text{ni}}$ value. Figure 6 shows that

the cutoff introduces a divergence in b_3 . This divergence arises because the cutoff alters the high-temperature behavior of Δb_3 , which implies that the divergencies of b_3^{ref} and Δb_3 no longer cancel. Importantly, b_3 is converged in the low-temperature (large $\tilde{\omega}$) regime even for a relatively small cutoff. This allows us to use the converged low-temperature tail to constrain b_3 in the high-temperature regime. Extrapolating b_3 (calculated using a cutoff of 9) to the high-temperature limit, we find $b_3^{(0)} \approx -0.068(1)$, which deviates by less than 2% from the exact value. The validity of the employed extrapolation scheme crucially hinges on the fact that the functional form of b_3 changes “predictably” as $\tilde{\omega}$ changes from the low- to the medium- to the high-temperature regime. For example, if b_3 changed sign in the medium- or high-temperature regime, as is the case for the coefficient $b_{2,1}$ that characterizes the behavior of two identical fermions and one lighter fermion (with a mass ratio from 3.11 to 8.62) [29], the extrapolation employed above would predict the incorrect high-temperature limit of $b_{2,1}$.

The interaction piece Δb_4 of the fourth-order virial coefficient can be expressed analogously to Δb_3 . In particular, we write the energies at unitarity in terms of the $s_{L,\nu}$ (see Sec. III and the supplemental material for a listing of the $s_{L,\nu}$ values) and perform, as in the three-body case above, the sum over the hyperradial quantum number q analytically. Since both natural and unnatural parity states of the four-body systems are affected by the s -wave interactions, the $s_{L,\nu}$ values corresponding to both natural and unnatural parity states need to be included when evaluating Δb_4 . The reference piece b_4^{ref} diverges as

$$b_4^{\text{ref}} = \frac{-1}{2}\tilde{\omega}^{-6} + \frac{3}{16}\tilde{\omega}^{-4} - \frac{1+64b_3^{(0)}}{32}\tilde{\omega}^{-3} - \frac{149}{3840}\tilde{\omega}^{-2} + \frac{1+64b_3^{(0)}-512b_3^{(2)}}{256}\tilde{\omega}^{-1} \quad (20)$$

in the high-temperature limit. This divergence must be cancelled by a divergence of Δb_4 of opposite sign.

Dash-dot-dotted, dash-dotted and dashed lines in Fig. 7 show b_4 at unitarity obtained by using the full expression for b_4^{ref} and by limiting the sums over ν and L in Δb_4 such that $s_{L,\nu} \leq 11/2$, $\leq 15/2$ and $\leq 19/2$, respectively. For the largest cutoff, our calculation includes 169 and 89 $s_{L,\nu}$ values associated with shifted states [not counting the $(2L+1)$ -multiplicity] of the harmonically trapped (2,2) and (3,1) systems with zero-range interactions, respectively. Figure 7 shows that b_4 is negative in the low-temperature (large $\tilde{\omega}$) regime and that neither b_4 nor its first or second derivatives with respect to $\tilde{\omega}$ change sign in the regime where b_4 is converged. This motivates us to extrapolate the converged part of b_4 to the medium- and high-temperature regime (see dotted line in Fig. 7), yielding $b_4^{(0)} = -0.0020(5)$.

The LDA predicts that the virial coefficient b_n^{hom} of the homogeneous system is related to the high-temperature limit of the n th order virial coefficient of the trapped

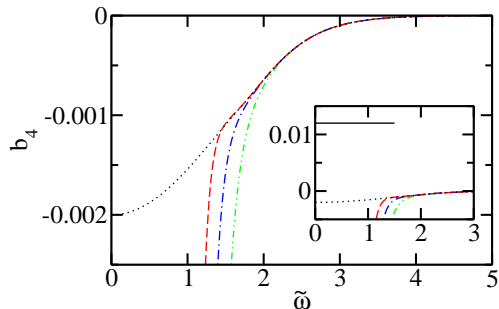


FIG. 7: (Color online) Virial coefficient b_4 of the trapped two-component Fermi gas at unitarity as a function of the inverse temperature $\tilde{\omega}$. The dash-dot-dotted, dash-dotted and dashed lines show b_4 obtained by limiting $s_{L,\nu}$ to be smaller than $11/2$, $15/2$ and $19/2$, respectively. The dotted line shows our attempt to extrapolate to the high-temperature limit; this extrapolation assumes that b_4 changes “predictably” from the low- to the medium- to the high-temperature regime. The inset shows the same data as the main figure. In addition, the solid horizontal line shows the high-temperature limit $b_4^{(0)}$ determined by applying the LDA to the fourth-order virial coefficient predicted for the homogeneous system [26].

system via [23]

$$b_n^{\text{hom}} = n^{3/2} b_n^{(0)}. \quad (21)$$

Application to our extrapolated $b_4^{(0)}$ yields $b_4^{\text{hom}} = -0.016(4)$. This value for the homogeneous system differs in both sign and magnitude from the values $b_4^{\text{hom}} = +0.096(15)$ [26] and $b_4^{\text{hom}} = +0.065(10)$ [27] determined from experimental data. These experimental values have been found to be consistent with the equation of state determined by a diagrammatic path integral Monte Carlo approach [28]. Given the disagreement between our value and that reported in the literature, we speculate that the fourth-order virial coefficient of the trapped system changes sign in the medium- or high-temperature limit, implying that the applied extrapolation scheme does not predict the correct medium- and/or high-temperature behavior of b_4 . If this conclusion is correct, it would follow that the determination of the medium- and high-temperature behavior of the fourth-order virial coefficient of the trapped systems requires, if determined via the microscopic energy spectra, knowledge of large portions of the energy spectra of the (2,2) and (3,1) systems. This suggests that other approaches, based on Feynman diagrams or based on simulating the finite temperature behavior directly numerically, may be more suitable than the approach pursued here for determining the temperature-dependence of b_4 .

We also analyzed the low-temperature tail of b_5 . Using the (3,2) and (4,1) energies from the supplemental material, we find that the fifth-order virial coefficient of the trapped Fermi gas at unitarity is positive

in the low-temperature limit. High precision measurements of the equation of state in the high-temperature regime might reveal if b_5 changes sign as a function of temperature. More generally, we find that the low-temperature limit of b_n at unitarity is fully determined by the low-temperature behavior of b_2 and Q_1 . To arrive at this result, we derive explicit expressions for Δb_n and b_n^{ref} for $n \leq 20$, and determine the low-temperature behavior of all terms that enter into Δb_n and b_n^{ref} . Using the ground state energies at unitarity for trapped two-component Fermi gases with up to $n = 20$ (with $|n_1 - n_2| = 0$ or 1) [6], we find that Δb_n falls off faster than b_n^{ref} with decreasing T , thus allowing us to obtain analytical expressions for the leading order low-temperature behavior of b_n : $b_{2n} \rightarrow \exp[i\pi(n-1)] \exp[-(2n-3/2)\tilde{\omega}]/(2n)$ and $b_{2n+1} \rightarrow \exp(i\pi n) \exp(-2n\tilde{\omega})$ for $n = 1, 2, \dots$. Thus, the sign of b_n in the low-temperature regime is $+, -, -, +, +, -, -, +, +, \dots$ for $n = 2, 3, 4, 5, 6, 7, 8, 9, 10, \dots$. For $n = 2 - 5$, we have checked that these analytical predictions agree with our numerically determined virial coefficients in the low-temperature regime. While the sign of b_n in the low-temperature regime may not allow one to draw conclusions about $b_n^{(0)}$, it is interesting, at least from a theoretical point of view, that the sign and functional form of b_n in the low-temperature regime are fully determined by Q_1 and b_2 .

V. SUMMARY

This paper considered the energy spectra of small trapped two-component Fermi gases with vanishing and finite angular momentum as well as natural and unnatural parity. Large portions of the energy spectra of the (2,2) and (3,1) systems at unitarity were determined as a function of the range of the underlying two-body model potential and extrapolated to the zero-range limit. The extrapolated zero-range energies are expected to be universal, i.e., independent of the underlying Gaussian model potential. Portions of the energy spectra of the (3,2) and (4,1) systems at unitarity were also determined. The energies were obtained by solving the relative Schrödinger equation using the stochastic variational approach. Compact expressions for the relevant matrix elements were presented in the appendix.

The (2,2) and (3,1) energies at unitarity were then used to determine the low-temperature behavior of the fourth-order virial coefficient b_4 of the trapped Fermi gas. The high-temperature limit of the fourth-order virial coefficient enters into the universal virial equation of state. The present study suggests that much larger portions of the microscopic energy spectra are needed to predict the high-temperature limit of b_4 . In our view this is unfortunate. Despite this, we believe that the analysis presented illuminates important characteristics relevant to the determination of the virial coefficients.

We gratefully acknowledge support by the ARO. KMD

and DB acknowledge hospitality of the INT where part of this work was conducted. We also gratefully acknowledge communication by the MIT-Amherst collaboration prior to publication of Refs. [27, 28].

Appendix A: Matrix elements

This appendix summarizes the expressions for the overlap, kinetic energy, trap potential, and interaction potential matrix elements for states with natural parity (any L) and unnatural parity ($L > 0$). For notational simplicity, we omit the subscripts of the matrix \underline{A}_k and the vectors \vec{u}_{1k} and \vec{u}_{2k} , and consider the matrix elements between the unsymmetrized basis functions ψ and ψ' characterized by $(\underline{A}, \vec{u}_1, \vec{u}_2)$ and $(\underline{A}', \vec{u}'_1, \vec{u}'_2)$, respectively [see Eq. (5) of Sec. II]. The matrix elements have been derived in the literature [32–37] and are summarized here for completeness.

Before providing explicit expressions for the matrix elements, we introduce a number of auxiliary quantities that are utilized in Subsecs. A 1 and A 2. The product of ψ' and ψ can be conveniently written in terms of the matrix \underline{B} ,

$$\underline{B} = \underline{A}' + \underline{A}. \quad (\text{A1})$$

We further define the scalars C and ρ_{ij} ($i, j = 1$ or 2),

$$C = \left(\frac{(2\pi)^{n-1}}{\det(\underline{B})} \right)^{3/2} \rho_{11}^{L-2} \quad (\text{A2})$$

and

$$\rho_{ij} = (\vec{u}'_i)^T \underline{B}^{-1} \vec{u}_j; \quad (\text{A3})$$

note that the order of the primed and unprimed vectors \vec{u}'_i and \vec{u}_j matters. We further define the scalars R and S_{ij} ($i, j = 1$ or 2),

$$R = 3\text{Tr}(\underline{B}^{-1} \underline{A} \underline{A} \underline{A}') \quad (\text{A4})$$

and

$$S_{ij} = (\vec{u}'_i)^T \underline{B}^{-1} \underline{A} \underline{A} \underline{A}' \underline{B}^{-1} \vec{u}_j, \quad (\text{A5})$$

where the diagonal elements of the matrix \underline{A} are given by the inverse of the masses associated with the Jacobi vectors and the off-diagonal elements of \underline{A} are zero. In Eq. (A4), Tr denotes the trace operator. The scalars $\tilde{R}^{(pq)}$ and $\tilde{S}_{ij}^{(pq)}$ ($p = 1, \dots, n$ and $q = p+1, \dots, n$) have a similar structure to R and S_{ij} ,

$$\tilde{R}^{(pq)} = 3\text{Tr}(\underline{B}^{-1} \underline{Q}^{(pq)}) \quad (\text{A6})$$

and

$$\tilde{S}_{ij}^{(pq)} = (\vec{u}'_i)^T \underline{B}^{-1} \underline{Q}^{(pq)} \underline{B}^{-1} \vec{u}_j. \quad (\text{A7})$$

The matrix $\underline{Q}^{(pq)}$ is defined as

$$\underline{Q}^{(pq)} = \vec{\omega}^{(pq)} \left(\vec{\omega}^{(pq)} \right)^T, \quad (\text{A8})$$

where $\vec{\omega}^{(pq)}$ is the $(n-1)$ -dimensional vector that relates the distance vectors \vec{r}_{pq} to the Jacobi vectors $\vec{x} = (\vec{\rho}_1, \dots, \vec{\rho}_{n-1})$,

$$\vec{r}_{pq} = \left(\vec{\omega}^{(pq)} \right)^T \vec{x}. \quad (\text{A9})$$

Lastly, we define the total mass M_{tot} ,

$$M_{\text{tot}} = \sum_{p=1}^n m_p. \quad (\text{A10})$$

1. Natural parity

For natural parity states, we use $l_1 = L$ and $l_2 = 0$ in Eq. (5), which implies that ψ' and ψ are independent of \vec{u}'_2 and \vec{u}_2 , respectively. In the following, we assume that ψ' and ψ are characterized by the same L and Π values. Under these assumptions the overlap matrix element is given by

$$\langle \psi' | O | \psi \rangle = N_L^{\text{nat}} C \rho_{11}^2, \quad (\text{A11})$$

where N_L^{nat} is a L -dependent constant that enters into all matrix elements and thus cancels when calculating expectation values. The kinetic energy matrix element reads

$$\langle \psi' | T^{\text{rel}} | \psi \rangle = N_L^{\text{nat}} \frac{\hbar^2}{2} C (R \rho_{11} + 2L S_{11}) \rho_{11}. \quad (\text{A12})$$

The matrix element for the trapping potential reads

$$\langle \psi' | V_{\text{trap}}^{\text{rel}} | \psi \rangle = N_L^{\text{nat}} \sum_{p=1, q>p}^n \frac{1}{2} \left(\frac{m_p m_q}{M_{\text{tot}}} \right) \Omega^2 C \times \left(\tilde{R}^{(pq)} \rho_{11} + 2L \tilde{S}_{11}^{(pq)} \right) \rho_{11}. \quad (\text{A13})$$

Lastly, the interaction matrix element for the Gaussian potential can be written as

$$\langle \psi' | V_{\text{int}} | \psi \rangle = -V_0 \sum_{p=1}^{n_1} \sum_{q=n_1+1}^n \langle \psi' | \exp[-r_{pq}^2 / (2r_0^2)] | \psi \rangle. \quad (\text{A14})$$

The expression for the matrix element $\langle \psi' | \exp[-r_{pq}^2 / (2r_0^2)] | \psi \rangle$ reduces to that for the overlap matrix element if the matrices \underline{A}' and \underline{A} are replaced by $\underline{A}' + \underline{Q}^{(pq)} / (2r_0^2)$ and $\underline{A} + \underline{Q}^{(pq)} / (2r_0^2)$, respectively.

2. Unnatural parity ($L > 0$)

For unnatural parity states with $L > 0$, we use $l_1 = L$ and $l_2 = 1$ in Eq. (5). In the following, we assume that ψ' and ψ are characterized by the same L and Π values. Under these assumptions the overlap matrix element is given by

$$\langle \psi' | O | \psi \rangle = N_L^{\text{unnat}} C \rho_{11} (\rho_{11} \rho_{22} - \rho_{12} \rho_{21}), \quad (\text{A15})$$

where N_L^{unnat} is a L -dependent constant that enters into all matrix elements and thus cancels when calculating expectation values. The kinetic energy matrix element reads

$$\begin{aligned} \langle \psi' | T^{\text{rel}} | \psi \rangle = N_L^{\text{unnat}} \frac{\hbar^2}{2} C \\ \{ [R\rho_{11} + 2(L-1)S_{11}] (\rho_{11}\rho_{22} - \rho_{12}\rho_{21}) + \\ 2\rho_{11} (\rho_{11}S_{22} + \rho_{22}S_{11} - \rho_{12}S_{21} - \rho_{21}S_{12}) \}. \quad (\text{A16}) \end{aligned}$$

The matrix element for the trapping potential reads

$$\begin{aligned} \langle \psi' | V_{\text{trap}}^{\text{rel}} | \psi \rangle = N_L^{\text{unnat}} \sum_{p=1, q>p}^n \frac{1}{2} \left(\frac{m_p m_q}{M_{\text{tot}}} \right) \Omega^2 C \times \\ \{ [\tilde{R}^{(pq)} \rho_{11} + 2(L-1)\tilde{S}_{11}^{(pq)}] (\rho_{11}\rho_{22} - \rho_{12}\rho_{21}) + \\ 2\rho_{11} (\rho_{11}\tilde{S}_{22}^{(pq)} + \rho_{22}\tilde{S}_{11}^{(pq)} - \rho_{12}\tilde{S}_{21}^{(pq)} - \rho_{21}\tilde{S}_{12}^{(pq)}) \} \quad (\text{A17}) \end{aligned}$$

As in the natural parity case, the expression for the interaction matrix element for the Gaussian potential can be related to that of the overlap matrix element by making the appropriate substitutions.

-
- [1] D. Blume, arXiv:1111.0941 (to appear in Rep. Prog. Phys.).
 - [2] C. Chin, R. Grimm, P. Julienne, and E. Tiesinga, Rev. Mod. Phys. **82**, 1225 (2010).
 - [3] S. Giorgini, L. P. Pitaevskii, and S. Stringari, Rev. Mod. Phys. **80**, 1215 (2008).
 - [4] F. Werner and Y. Castin, Phys. Rev. Lett. **97**, 150401 (2006).
 - [5] J. von Stecher and C. H. Greene, Phys. Rev. Lett. **99**, 090402 (2007).
 - [6] D. Blume, J. von Stecher and C. H. Greene, Phys. Rev. Lett. **99**, 233201 (2007).
 - [7] J. P. Kestner and L.-M. Duan, Phys. Rev. A **76**, 033611 (2007).
 - [8] I. Stetcu, B. R. Barrett, U. van Kolck, and J. P. Vary, Phys. Rev. A **76**, 063613 (2007).
 - [9] J. von Stecher, C. H. Greene, and D. Blume, Phys. Rev. A **77**, 043619 (2008).
 - [10] Y. Alhassid, G. F. Bertsch, and L. Fang, Phys. Rev. Lett. **100**, 230401 (2008).
 - [11] D. Blume and K. M. Daily, Phys. Rev. A **80**, 053626 (2009).
 - [12] K. M. Daily and D. Blume, Phys. Rev. A **81**, 053615 (2010).
 - [13] J. Rotureau, I. Stetcu, B. R. Barrett, M. C. Birse, and U. van Kolck, Phys. Rev. A **82**, 032711 (2010).
 - [14] D. Blume and K. M. Daily, C. R. Physique **12**, 86 (2011).
 - [15] S. Tan, Phys. Rev. Lett. **107**, 145302 (2011).
 - [16] C. N. Gilbreth and Y. Alhassid, arXiv:1108.2687.
 - [17] S. Bour, X. Li, D. Lee, U.-G. Meißner, and L. Mitas, Phys. Rev. A **83**, 063619 (2011).
 - [18] S. T. Rittenhouse, J. von Stecher, J. P. D'Incao, N. P. Mehta, and C. H. Greene, J. Phys. B **44**, 172001 (2011).
 - [19] J. von Stecher and C. H. Greene, Phys. Rev. A **80**, 022504 (2009).
 - [20] T.-L. Ho and E. J. Mueller, Phys. Rev. Lett. **92**, 160404 (2004).
 - [21] T.-L. Ho, Phys. Rev. Lett. **92**, 090402 (2004).
 - [22] G. Rupak, Phys. Rev. Lett. **98**, 090403 (2007).
 - [23] X.-J. Liu, H. Hu, and P. D. Drummond, Phys. Rev. Lett. **102**, 160401 (2009).
 - [24] D. B. Kaplan and S. Sun, Phys. Rev. Lett. **107**, 030601 (2011).
 - [25] X. Leynoras, Phys. Rev. A **84**, 053633 (2011).
 - [26] S. Nascimbène, N. Navon, K. J. Jiang, F. Chevy, and C. Salomon, Nature **463**, 1057 (2010).
 - [27] M. J. H. Ku, A. T. Sommer, L. W. Cheuk, and M. W. Zwierlein, arXiv:1110.3309.
 - [28] K. Van Houcke, F. Werner, E. Kozik, N. Prokof'ev, B. Svistunov, M. Ku, A. Sommer, L. W. Cheuk, A. Schirrotzek, and M. W. Zwierlein, arXiv:1110.3747.
 - [29] K. M. Daily and D. Blume, Phys. Rev. A **85**, 013609 (2012).
 - [30] See supplementary material at XXX [web link, to be inserted by publisher].
 - [31] T. Busch, B.-G. Englert, K. Rzǎżewski, and M. Wilkens, Foundations of Phys. **28**, 549 (1998).
 - [32] Y. Suzuki and K. Varga, *Stochastic Variational Approach to Quantum Mechanical Few-Body Problems* (Springer Verlag, Berlin, 1998).
 - [33] K. Varga and Y. Suzuki, Phys. Rev. C **52**, 2885 (1995).
 - [34] K. Varga, Y. Suzuki, and J. Usukura, Few-Body Syst. **24**, 81 (1998).
 - [35] Y. Suzuki, J. Usukura and K. Varga, J. Phys. B **31**, 31 (1998).
 - [36] Y. Suzuki and J. Usukura, Nuclear Instruments and Methods in Physics Research B **171**, 67 (2000).
 - [37] Y. Suzuki, W. Horiuchi, M. Orabi, and K. Arai, Few-Body Syst. **42**, 33 (2008).
 - [38] S. Aoyama, K. Arai, Y. Suzuki, P. Descouvemont, and D. Baye, arXiv:1106.3391.
 - [39] The states are counted separately for each L^Π symmetry. In counting the states, we do include the unshifted states but we do not account for the $2L + 1$ degeneracy of the energies (see column 1 of Table 1 for the state number).
 - [40] F. Werner and Y. Castin, Phys. Rev. A **74**, 053604 (2006).
 - [41] D. A. McQuarrie, *Statistical Mechanics*, University Sci-

- ence Books, California, 2000.
- [42] K. Huang, *Statistical Mechanics, 2nd Ed.* (John Wiley and Sons, Inc., New York, 1963).
- [43] X.-J. Liu and H. Hu, Phys. Rev. A **82**, 043626 (2010).